

ARTICLE OPEN



Cytotoxicity survey of commercial graphene materials from worldwide

Ritika Malhotra^{1,12}, Christian Eberhard Halbig^{2,3,12}, Yu Fan Sim¹, Chwee Teck Lim^{4,5,6}, David Tai Leong^{7,8}, A. H. Castro Neto^{2,9,10}, Slaven Garaj^{2,5,9,10} and Vinicius Rosa^{1,2,9,11}

Graphene and other 2D materials are having a profound impact on science and technology. Unfortunately, progress in this area has not been followed by strict quality controls and toxicity benchmarks. Herein, we report a survey of the cytotoxicity of 36 products nominally labeled as “graphene.” These are available from suppliers worldwide and synthesized through various techniques. Detailed characterization suggests that these products represent a heterogeneous class of materials with varying physicochemical properties and a noticeable quantity of contaminants. We demonstrate that the cellular toxicity of these products is not related to a particular characteristic of graphene; rather, it is fundamentally determined by the presence of impurities in the commercially available graphene family materials tested.

npj 2D Materials and Applications (2022)6:65; <https://doi.org/10.1038/s41699-022-00330-8>

INTRODUCTION

The unique properties of graphene have the potential to support the development of the next generation of composites, electronics, membranes, energy storage devices, drug delivery systems, implantable materials, etc.^{1–4}. An exclusive graphene industry was already emerging even before the standards for quality and toxicity control had been established. Previous study has shown that most of the graphene products available in the market are poorly characterized ‘black powders’ that do not adhere to appropriate standards⁵. Even more pressing is the question concerning the toxicity of the globally available graphene, especially when graphene-based products are considered for medical and consumer use.

The current literature presents conflicting results regarding the cytocompatibility-related character of graphene. “The dose makes the poison”, and the physiochemical characteristics of the material can play critical roles in cytocompatibility⁶. Contamination can occur at many different stages of graphene production due to the diversity of precursors and manufacturing processes^{7–10}. Several methods have been developed to produce graphene, and some of these involve the use of chemicals that are not biocompatible and can cause adverse health effects^{10–14}. Moreover, the graphene obtained industrially is multi-layered with a broad distribution of dimensions which can also impact its toxicity^{10,12,15–17}. Finally, harsh conditions imposed on the graphitic precursors during the industrial process, the presence of intermetallic impurities and certain amounts of permanent structural defects in the hexagonal carbon framework can also impact graphene’s toxicity^{8,9,18,19}. The graphene sold worldwide contains a wide span of particle sizes, number of layers, different types of structural defects, and are contaminated with extrinsic material^{5,10,14,20}. Figure 1a illustrates in a simplified manner some of the named aspects of graphene.

These can confer either cytotoxicity or cytocompatibility character depending on the mode of use and the dosage^{21–28}. Thus, there is a growing understanding that the toxic character of each graphene product must be evaluated individually.

We investigated the toxicity of graphene products available commercially and correlated their cytotoxicity to the material’s physical and chemical characteristics. We examined 36 commercially available graphene products and found a surprisingly large variability in cytotoxicity, from harmless to highly toxic. The graphene products were investigated as received from suppliers, without any additional processing or modifications that could skew in vitro toxicity results. To understand these results, we have performed a detailed characterization of these materials. Our study suggests that over 35% of the graphene products contain highly defective graphene; we observed the presence of organic and/or inorganic impurities in almost all the samples. Our results prompt the conclusion that a product’s cytotoxicity cannot be related to any characteristic of graphene alone, but it is determined by the contaminants present.

RESULTS

Nominal graphene materials (NGMs) characterization

We refer to products in this study as nominal graphene materials (NGMs), as they represent heterogenous class of materials with different chemical components and different physiochemical properties of graphitic portion. The obtained NGMs consist of graphitic materials with different macroscopical appearance: some of them are dense and grained with a metallic aspect, while others are extremely soft, voluminous, and deep black (Supplementary Fig. 1), or in-between the outlined range. This already indicates

¹Faculty of Dentistry, National University of Singapore, Singapore, Singapore. ²Centre for Advanced 2D Materials, National University of Singapore, Singapore, Singapore. ³Institute of Chemistry and Biochemistry, Freie Universität Berlin (FU-Berlin), Berlin, Germany. ⁴Mechanobiology Institute, National University of Singapore, Singapore, Singapore. ⁵Department of Biomedical Engineering, National University of Singapore, Singapore, Singapore. ⁶Institute for Health Innovation and Technology, National University of Singapore, Singapore, Singapore. ⁷Department of Chemical and Biomolecular Engineering, College of Design and Engineering, National University of Singapore, Singapore, Singapore. ⁸NUS Graduate School for Integrative Sciences & Engineering, National University of Singapore, Singapore, Singapore. ⁹Department of Materials Science and Engineering, College of Design and Engineering, National University of Singapore, Singapore, Singapore. ¹⁰Department of Physics, Faculty of Science, National University of Singapore, Singapore, Singapore. ¹¹ORCHIDS: Oral Care Health Innovations and Designs Singapore, National University of Singapore, Singapore, Singapore. ¹²These authors contributed equally: Ritika Malhotra, Christian Eberhard Halbig. ✉email: c2dhead@nus.edu.sg; slaven@nus.edu.sg; vini@nus.edu.sg

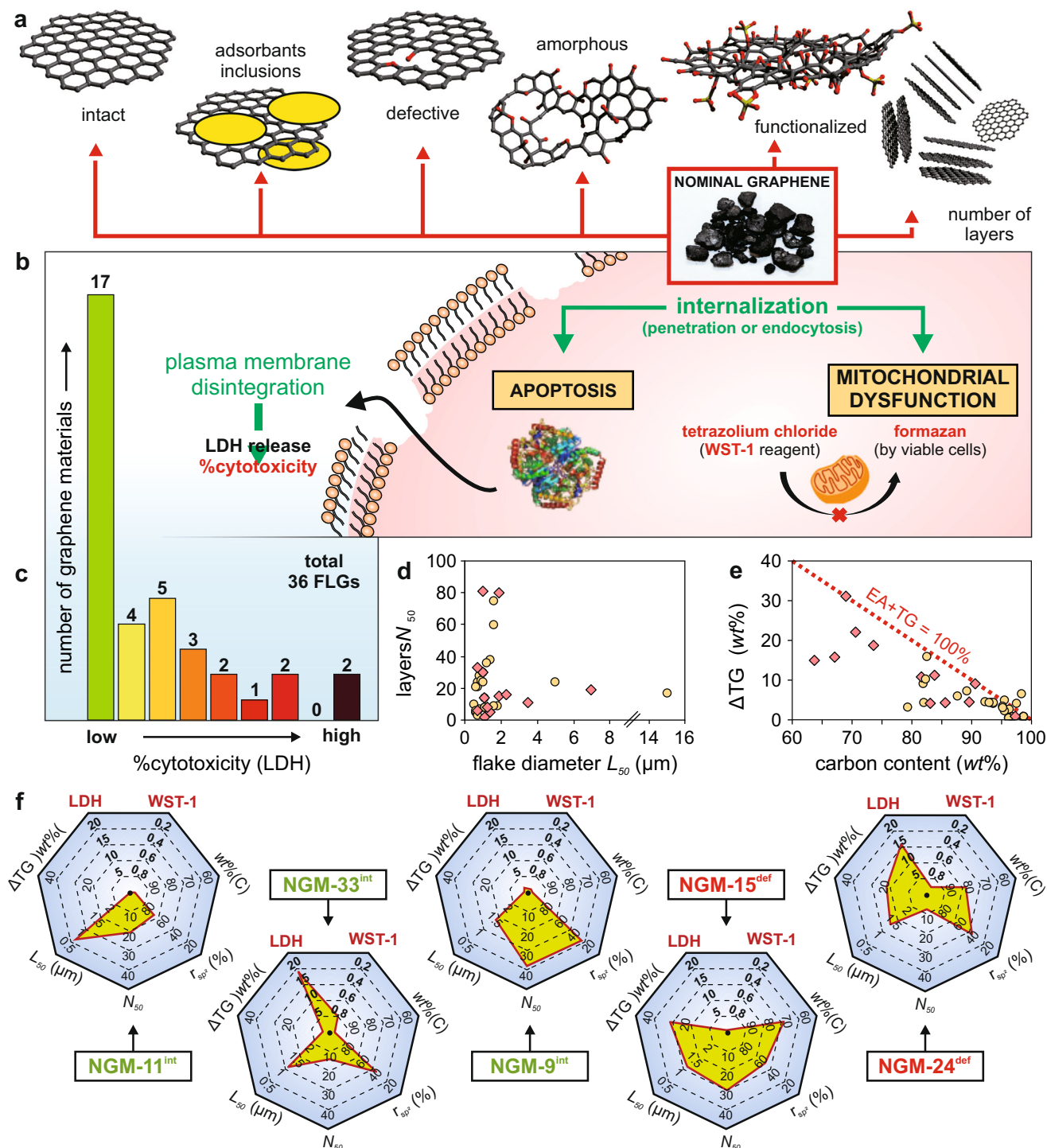


Fig. 1 Overview of possible components of nominal graphene materials (NGMs). **a** From left to right: graphene with and without in-plane defects; adsorbates and inclusions (yellow circles); slightly defective graphene and graphene dominated by extensive defects like holes or oxo-functional groups; highly functionalized graphene oxide; graphene with different number of layers. **b** Scheme of the internalization of graphene samples by cells and potential toxic outcomes measured by WST-1 and LDH. **plasma membrane disintegration** leads to **LDH release** and **%cytotoxicity**. **internalization (penetration or endocytosis)** leads to **APOPTOSIS** and **MITOCHONDRIAL DYSFUNCTION**. Mitochondrial dysfunction is measured using **tetrazolium chloride (WST-1 reagent)** and **formazan (by viable cells)**. **c** Distribution of cytotoxicity measured by LDH release. **d** Median flake diameter L_{50} vs. median number of layers N_{50} . **e** Proportion of carbon content, $wt\%(C)$, measured by elemental analysis, vs. thermogravimetric mass loss ΔTG in the range from 100 °C to 800 °C. The dashed red line represents the 100% line of the sum of carbon content $wt\%(C)$ and mass loss. Intact graphene (NGM^{int}) is represented by yellow circles, defective graphene (NGM^{def}) by red diamonds in both diagrams. **f** Illustration of performance heptagrams for five different NGMs, representing their physiochemical properties and toxicity. Samples **NGM-11^{int}**, **NGM-33^{int}**, and **NGM-9^{int}** are high graphitic samples of good quality but have different toxicity profile. **NGM-15^{def}** and **NGM-24^{def}** are very disordered, otherwise very similar, but one is toxic while the other is harmless.

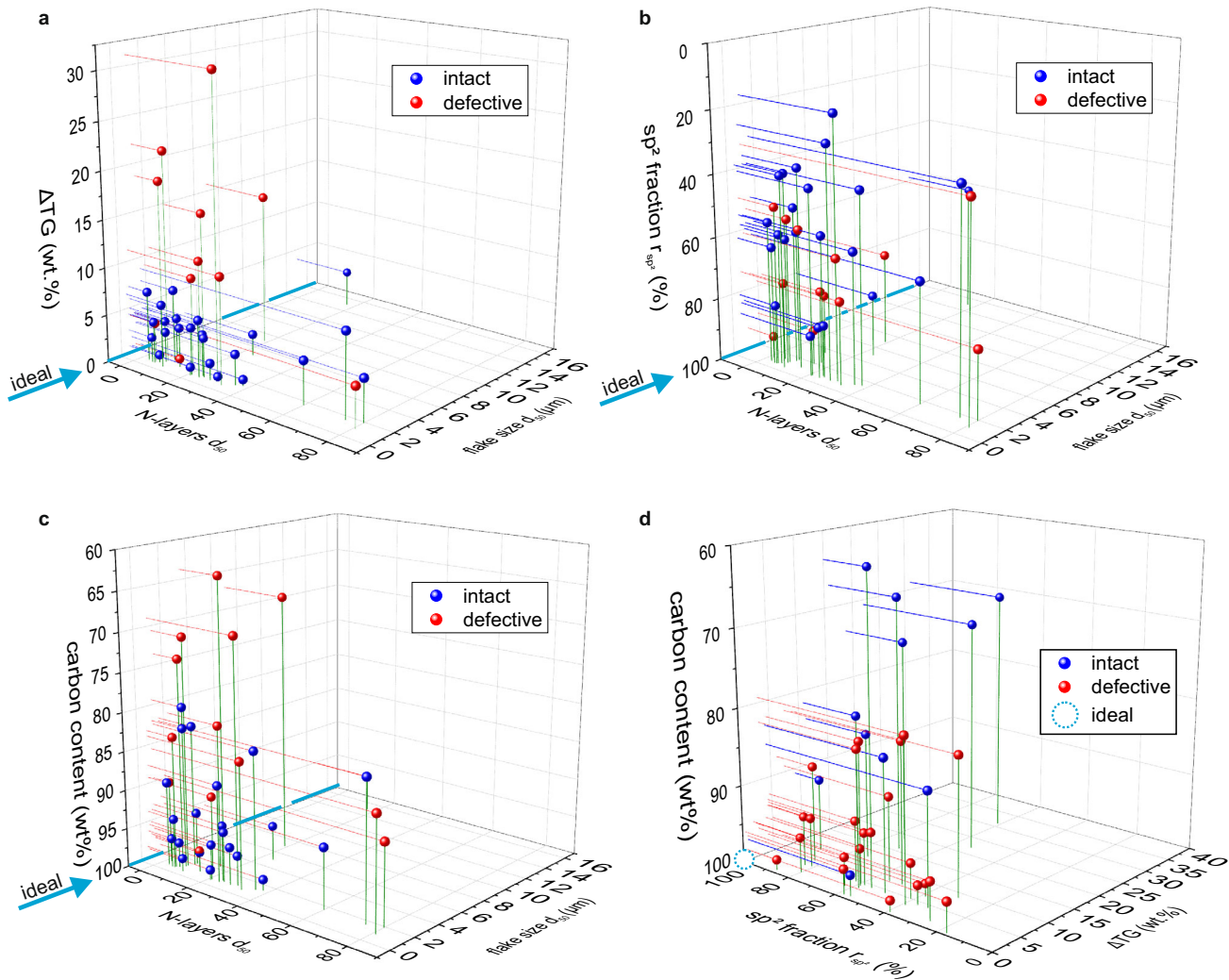


Fig. 2 Characterization of nominal graphene materials (NGM). Three-dimensional plots of the physiochemical properties defining the quality of graphene according to Wick et al., with **a** ΔTG . **b** $r(sp^2)$; and **c** $wt\%(C)$. **d** 3-Dimensional plot comparing all three before-named measures for the degree of functionalization. A blue bar or blue circle indicates the direction of “ideal” graphene: The more the points are located at this axis or point, respectively, the more ideal the structure³¹.

that their physio-chemical properties differ strongly from what we will consequently outline in the following section in greater detail.

Flake thickness, graphene fraction, and lateral size

Using optical microscopy, Raman spectroscopy, and atomic force microscopy (AFM), we found that the NGMs consist of few- and multi-layered materials (Figs. 1d, 2, Supplementary Fig. 2a). In 2017, the ISO defined the concepts of bilayer and few-layer graphene (FLG, with three to 10 layers), in accordance with the definitions detailed by the Editorial Board of the Journal *Carbon* and Wick et al.^{29–31}.

We define N_{50} and N_{90} as the 50th percentile (median value) and 90th percentile value of the distribution of the number of graphene layers of each material. $N_{50} \leq 10$ layers occurred, whereas the average N_{50} value was 23. None of the samples had N_{90} below 10 layers. The lowest value of N_{90} (13 layers) was found for two NGMs, and the next best N_{90} was equal to 31. Thus, we defined the graphene fraction (r_G) as a fraction of the flakes with $N_{50} \leq 10$, satisfying the definition of FLG. Most of the samples had $r_G < 10\%$, and only one sample had r_G of $\sim 50\%$. Similarly, the flakes' sizes were quantified for L_{50} and L_{90} as the median value

and 90th percentile. Most of the samples had L_{50} diameter, ranging between 0.5 and 15 μm (overall median value of 1.1 μm), and L_{90} varying between 1.5 μm and 100 μm (overall median of 5.4 μm).

The three-dimensional representation of physiochemical properties defining the quality of the graphene according to Wick et al. is presented in Fig. 2.

Defect density, carbon content, volatile, and sp^2 fractions

The quality of NGMs was analyzed through an evaluation of the intensities of the *D* and *G* mode (I_D/I_G) of recorded Raman spectra, and the density of defects (L_D) with respect to carbon atoms was calculated using a formula published by Lucchese, Cançado et al. (Supplementary Fig. 3, Supplementary Table 1)³². We separated all materials involved in the survey into two groups: intact (NGM^{int}) and defective dominated (NGM^{def}); the threshold was established as 1.3% defects ($I_D/I_G \sim 1.3$, and average length between two defects, $L_D \sim 1.42$ nm). For higher densities, the I_D/I_G becomes less precise with the ratio approximating values around ~ 1.0 , and densities of defects cannot be reliably calculated anymore in this defect-dominated regime³³. Nevertheless, 23 materials were almost intact and bear a low density of defects and were

consequently categorized as NGM^{int} , while the other 13 samples have a significantly disturbed carbon lattice and were thus labeled as NGM^{def} . From this group, three samples presented Raman spectra resembling amorphous carbon. Since defects in the hexagonal carbon structure can be not only permanent in-plane lattice defects such as vacancies, grain boundaries, and other non-hexagonal ring structures, but also sp^3 hybridized carbon with functional groups (cf. graphene oxide), we will have a differentiated evaluation of both groups in the following analysis.

Carbon content (wt%(C)) was determined via combustion elemental analysis (Supplementary Fig. 2b). Ideally, graphene should consist of pure carbon, but herein, NGMs presented wt%(C) varying widely between 63 and 98 wt%. From the 13 samples that presented wt%(C) > 92 wt%, only one was NGM^{def} . Notably, half of the 14 samples with wt%(C) ranging from 90 to 79 wt% were NGM^{def} . Finally, the five materials with the lowest wt%(C) ranging from 63 to 73 wt%, were all in the NGM^{def} group. Based on this outcome, it is feasible to note that a correlation between structural integrity and long-range order by means of Raman spectroscopy does not necessarily imply a high detected carbon content in the NGM and, consequently, high purity.

We characterized the thermal decomposition of NGMs using thermogravimetric analysis-mass spectroscopy (TGA-MS; 100 °C to 800 °C) to deduce the part of the non-carbon content that corresponds to functional groups, adsorbents, surfactants, and other contaminants (Supplementary Fig. 4a–d). Herein, 80% of the samples had ΔTG lesser than 12 wt%. The highest ΔTG values (31.1–9.1 wt%) were observed for the NGM^{def} group. The strong mass decay with increasing temperature may be related to thermal degradation at the large defect sites, as observed in humic substances and activated carbon, but unlikely from graphene oxide-like materials, as obligatory mass fragments with m/z 17, 18, 28, 44, 64 do not match the typical pattern or are negligible to absent (Supplementary Fig. 4e, Supplementary Table 1)³⁴. Interestingly, some NGM^{int} had $\Delta TG = 8.8$ wt%, while some NGM^{def} had negligible mass loss ($\Delta TG = 0.9$ wt%). This is an interesting observation, as high mass loss is typically associated with the cleavage of functional groups which can easily be detected by Raman spectroscopy, while the ideal graphene material without any defects should not experience any thermal decomposition. Furthermore, all NGMs presented a noticeable amount of fragment ions, with m/z ratios between 15 and 78 (Supplementary Table 1), indicating that all the NGMs contain contaminants which are not present in pristine graphite used as control (Supplementary Fig. 4f).

We identified that a certain amount of non-carbon material (cf. results from EA) failed to evaporate when heated up to 800 °C in TGA, which we will refer to as persistent inorganics (PIs). The precise proportion of carbon-to-inorganics in the volatile component ΔTG is unknown; hence, we defined a lower bound for the cases in which all the volatiles ΔTG are inorganics and an upper bound if all volatiles are carbon.

The fraction of sp^2 bounded carbon ($r(sp^2)$) was obtained from the deconvoluted intensities of XPS C1s core spectra with Shirley background correction (Supplementary Fig. 5)³⁵. For ideal graphene, the $r(sp^2)$ should be close to 100%, with only the edge carbon atoms and adventurous carbon slightly reducing the overall value, whereby other defects, functional groups, and organics reduce the overall $r(sp^2)$ significantly. The XPS is a surface-sensitive technique where the penetration of the photoelectrons is limited to a few nanometers³⁶; hence, it can detect contaminants and inclusions on flake surfaces regardless of its thickness. The $r(sp^2)$ ranged from 8.2 to 86.5%, with a median of 38.9% and a mean value of 41.4%. Interestingly, nine out of the ten lowest $r(sp^2)$ values were NGM^{int} , suggesting the presence of surface contaminants (e.g., adventitious carbon, solvent, or surfactant residues), as intact graphene should not have sp^3 hybridized carbon.

Washing of the samples for the removal of possible organic and inorganic adsorbents and inclusions was performed *via* repetitive centrifugation and the use of 1 M HCl, ethanol, chloroform, ethanol, 0.1 M KOH, and finally, six times washing with DI water in the listed order. Aside from the final wash with DI water, the incubation time and temperature for the NGM treatment were 60 °C for 2 h for each solvent or solution, respectively. Finally, the materials were dried at 80 °C at reduced pressure for two days using a common drying oven and membrane pump.

Toxicity profile

The cytotoxicity of the NGMs on L929 cell lines was determined using the following: (a) colorimetric measurement of mitochondrial dehydrogenase activity via the conversion of tetrazolium salt providing information about the cell viability (WST-1) and (b) assessment of the lactate dehydrogenase (LDH) activity following plasma membrane rupture, signifying cytotoxicity. Generally, NGMs with a high cell viability (WST-1) have low cytotoxicity (LDH) and vice versa, but owing to the different mechanisms of cellular toxicity, the correlation is not always perfect. As the toxicity is concentration-dependent⁶, we tested the effect of different NGM concentrations. The results from the highest concentration (50 µg/ml) were discarded, as it promoted the eradication of cells. Herein, the trends for 10 µg/ml were analogous to 25 µg/ml (Supplementary Figs. 6–8; Supplementary Table 1). A correlation coefficient value (r_s) < 0.3 indicates a poor correlation, while values between 0.3–0.5 and >0.5 indicate moderate and strong correlations, respectively. The statistical correlations are discussed in the following for all samples (combined, r_s^{com}) or for structural intact (r_s^{int}) or defective (r_s^{def}) materials separately, and a tabular overview of the correlation coefficients can be found in Table 1 and Supplementary Table 1.

The statistical correlations for WST-1 and LDH with NGMs' flake size (L_{50}) and number of layers (N_{50}) are indicated in Figs. 3, 4 and Table 1 (for 90-percentile values L_{90} and N_{90} see Supplementary Fig. 8). We observed a moderately positive correlation between the N_{50} and cell viability (WST-1 $r_s^{com} = 0.381$, $p < 0.05$), and a slight positive correlation between L_{50} and cytotoxicity (LDH $r_s^{com} = 0.405$, $p < 0.05$). Generally, we have not observed higher toxicity for NGM^{def} samples as compared with NGM^{int} (Figs. 3, 4). There was no significant correlation between the reduced cell viability for larger flake diameter (WST-1 $r_s^{def} = -0.427$, $p > 0.05$) and low graphene content (WST-1 $r_s^{def} = -0.473$, $p > 0.05$) for NGM^{def} . Despite this correlation, some NGM^{def} presented low toxicity while having large flakes or low graphene content (Figs. 1f, 3b, e, 4b, e). This suggests that the toxicity is not primarily determined by the density of lattice defects, flake thickness, or dimensions; rather, it is likely to be caused by the presence of contaminants.

Furthermore, there were no significant correlations were seen between properties like specific surface area (SSA), $r(sp^2)$ and analyzed measures of cell toxicity (SSA- WST-1 $r_s^{com} = 0.007$, $p > 0.05$; LDH $r_s^{com} = 0.110$, $p > 0.05$; $r(sp^2)$ - WST-1 $r_s^{com} = 0.099$, $p > 0.05$; LDH $r_s^{com} = -0.134$, $p > 0.05$). We also observed a moderate and significant correlation with the total carbon content (WST-1 $r_s^{com} = 0.499$, $p < 0.001$; LDH $r_s^{com} = -0.374$, $p < 0.05$), indicating that the non-carbon inclusions are frequent, but not the sole determinant of toxicity.

We observed no relevant correlation between the cytotoxicity and the physical or chemical properties of the graphene components of NGMs. These findings led us to conclude that the toxicity mostly arises from the different types of non-graphene contaminants in the samples. To corroborate the principle experiment, we washed six representative NGMs comprising of both, intact and defective samples with both high and low cytocompatibility, *via* consecutive washing with 1 M acid, ethanol, chloroform, 0.1 M lye, and finally DI water, throughout at 60 °C, to

Table 1. Spearman's correlation coefficients: combined (r_s^{com}), for NGM^{int} (r_s^{int}) and for NGM^{def} (r_s^{def}).

	WST-1 Correlation coefficient			LDH Correlation coefficient		
	Combined (r_s^{com})	NGM^{int} (r_s^{int})	NGM^{def} (r_s^{def})	Combined (r_s^{com})	NGM^{int} (r_s^{int})	NGM^{def} (r_s^{def})
Carbon (wt%(C))	0.499 **	0.547 **	0.373	-0.374*	-0.565**	0.175
sp^2 fraction, $r(sp^2)$ (%)	0.099	0.275	-0.137	-0.134	-0.207	0.329
Graphene fraction, r_G (%)	-0.233	-0.180	-0.473*	0.068	-0.013	0.466
ΔTG (wt%)	-0.204	-0.182	-0.118	0.085	0.143	-0.136
N Layers N_{50}	0.381*	0.370	0.472*	-0.221	-0.156	-0.476**
N Layers N_{90}	0.262	0.192	0.461**	-0.102	-0.035	-0.406*
Flake size L_{50} (μm)	-0.316	-0.271	-0.427*	0.405*	0.470*	0.168
Flake size L_{90} (μm)	0.156	0.180	0.225	0.107	0.115	-0.035
SSA (m^2/g)	-0.189	-0.09	-0.027	0.007	0.107	0.175

The correlation values of LDH are after exclusion of an outlier found in the dataset (highest value measured in the Y axis in Fig. 3). ** $p < 0.001$; * $p < 0.05$.

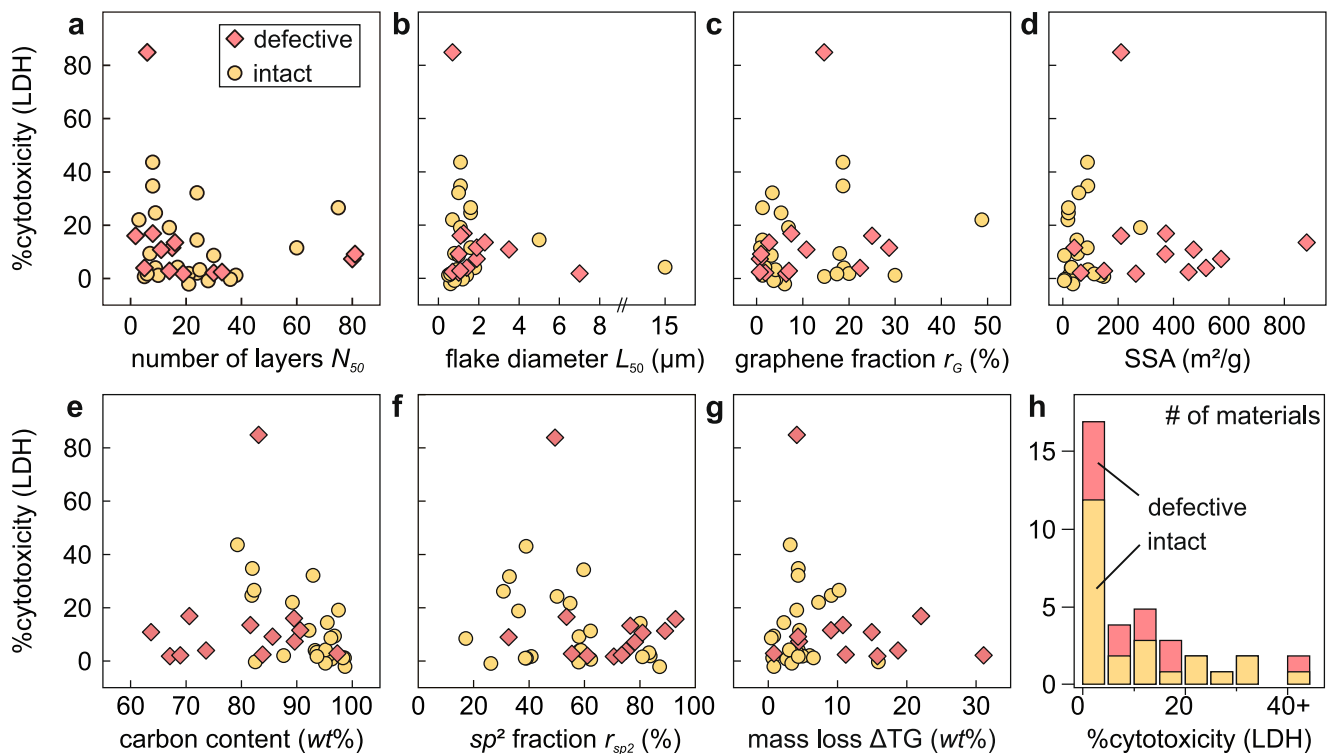


Fig. 3 Commercial graphene materials' properties induce varying %cytotoxicity responses in cells. Correlation analysis of %cytotoxicity (LDH release) stimulated by nominal graphene materials (NGM's) at $10 \mu\text{g}/\text{ml}$ concentration: **a** Median of number of layers N_{50} . **b** median flake diameter L_{50} . **c** Graphene content r_G . **d** Specific surface area (SSA) calculated by the Brunauer, Emmett, and Teller method (BET). **e** Carbon content wt%(C). **f** Fraction of sp^2 bounded carbon, $r(sp^2)$. **g** Thermogravimetric mass loss ΔTG in the 100°C to 800°C temperature range. **h** Representation of number of intact or defective NGMs to varying levels of %cytotoxicity. Intact graphene samples, NGM^{int} , are represented by yellow circles and defective graphene samples, NGM^{def} , are shown as red diamonds. The outlier (highest value measured in the Y axis) is shown only for reference and had not been included in the statistical analysis. The combined Spearman's correlation (r_s^{com}) and the significance (p -value) for each graph are presented in Table 1.

free the NGMs from potential impurities on the surface. Notably, there was no significant statistical difference in the cytotoxic character of highly cytocompatible graphene materials after washing (low cytotoxicity in Fig. 5, $p > 0.05$). However, there was a significant decrease in toxicity for most of the cytotoxic samples, analyzed after the washing procedures ($p < 0.05$). Collectively, these data suggest that the toxicity was due to non-graphene contaminants which may be present in the raw material or involved in the production process (Fig. 5a, b). Additional optimization in the washing protocol is warranted to further

improve the cytocompatible character of commercially available graphene materials.

Principal component and hierarchical cluster analysis

We have established the toxicity profile (i.e., the cell viability and %cytotoxicity reported as WST-1 and LDH respectively) of the NGMs using principal component analysis (PCA) and hierarchical cluster analysis (HCA). This was done to determine whether there is any relationship between the toxicity profile of NGM^{int} and NGM^{def} , independent of the properties analyzed. A PCA-biplot

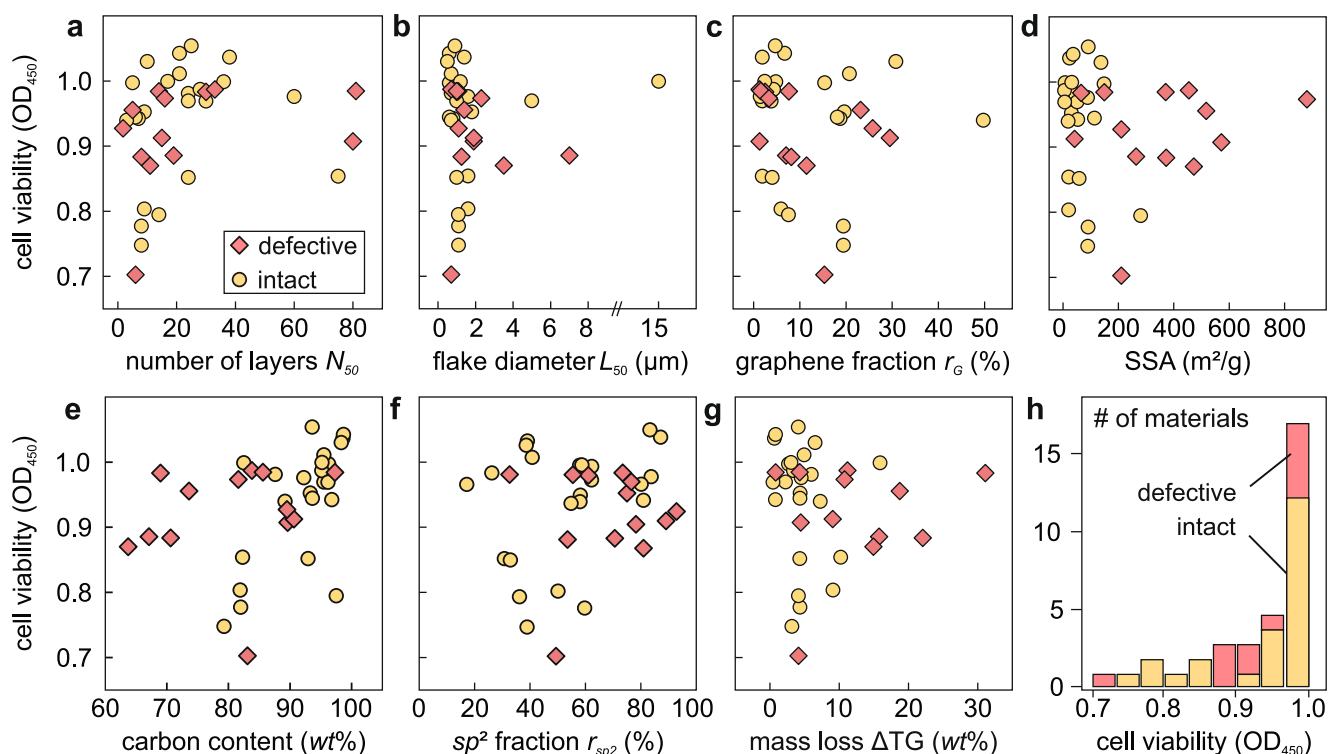


Fig. 4 Cell viability is simultaneously affected by several properties of commercial graphene materials. Correlation analysis of WST-1 (cell viability) stimulated by nominal graphene materials (NGMs) at 10 $\mu\text{g}/\text{ml}$ concentration: **a** median of number of layers N_{50} . **b** median flake diameter L_{50} . **c** graphene content r_G . **d** specific surface area (SSA) calculated by the Brunauer, Emmett, and Teller method (BET). **e** carbon content wt%. **f** Fraction of sp^2 bounded carbon, $r(sp^2)$. **g** thermogravimetric mass loss ΔTG in the 100 $^\circ\text{C}$ to 800 $^\circ\text{C}$ temperature range. **h** representation of number of intact or defective NGMs to varying levels of %cytotoxicity. Intact graphene samples, NGM^{int} , are represented by yellow circles and defective graphene samples, NGM^{def} , are shown as red diamonds. The combined Spearman's correlation (r_s^{com}) and the significance (p -value) for each graph are presented in Table 1.

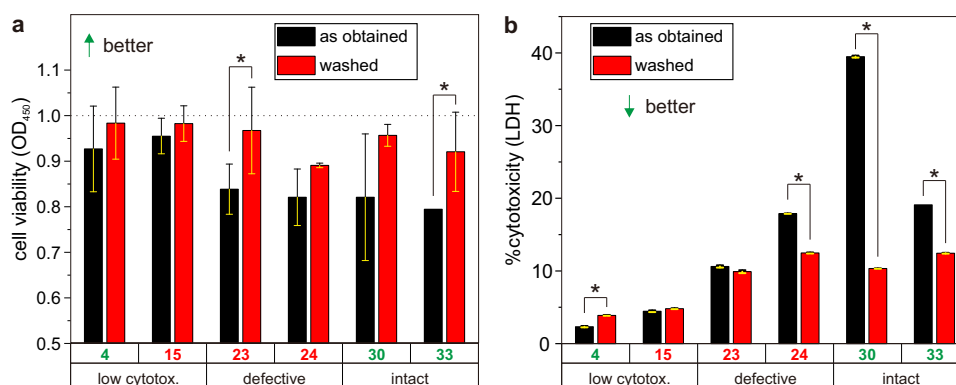


Fig. 5 Correlation between fraction of persistent inorganics (PI) and degrees of cytotoxicity. **a** Changes in cell viability, and **b** %cytotoxicity before and after consecutive ultrasound bath assisted washing with hot acid (1 M) and ethanol, chloroform, ethanol, lye (0.1 M), and finally, three times DI water at 60 $^\circ\text{C}$ for the removal of potential impurities. Similar concentrations (10 $\mu\text{g}/\text{ml}$) of the finally freeze-dried products were used. Samples in green and red denotes NGM^{int} and NGM^{def} respectively. *Denotes statistically significant difference between the samples ($p < 0.05$). Error bars represent standard deviation between three independent samples.

(scatter and loading plot) was constructed, in which the scatter points are the principal component (PC) scores of each sample, and the arrows represent the loading of each sample (i.e., the cell viability and cytotoxicity). The analysis computed two significant components: PC1 and PC2 that accounts for the highest and second highest variance probabilities in the dataset. In this analysis, the lower the PC1 score, the more cytotoxic is the material and vice-versa. Clearly, PC1 predominantly contributes (86.83%) to the total variation of the cell viability and cytotoxicity

(Fig. 6a). The scattered data in the PCA biplot are individual data points which suggests that three apparent clusters (block = NGM^{int} , open = NGM^{def}) are formed. The blue cluster represents the most cytocompatible materials (high WST-1) and slight overlaps with the red cluster, both dominated by NGM^{int} , indicating higher overall cell viability by the NGM^{int} . The materials from the green cluster presented high toxicity mainly induced by membrane damage (LDH release). Finally, an inspection of the loading plot clearly indicates that PC1 mainly

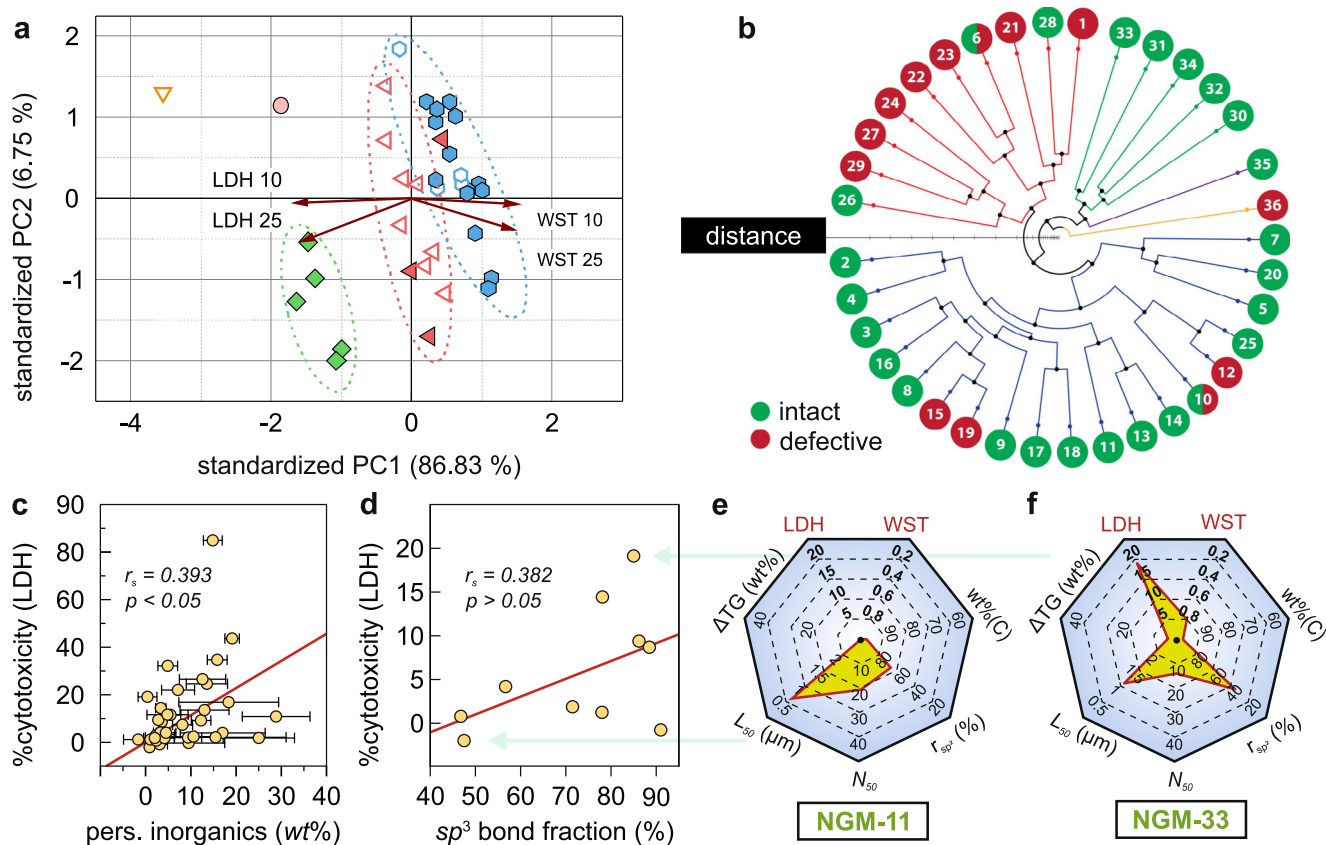


Fig. 6 Potential associations of tested properties of commercial nominal graphene materials and cell viability and membrane damage. **a** PCA-biplot (score and loading plot) from principal component analysis. Three apparent clusters can be seen from the PC scores of the samples. The solid scatter points are NGM^{int} and open scatter points are NGM^{def} . **b** HCA dendrogram. Vertical lines represent roots samples while horizontal lines represent similarities between samples. Two samples cannot be classified into either intact or defective graphene and are thus indicated with green/red circles. **c** Persistent inorganics; and **d** Fraction of sp^3 bonded carbon ($r(sp^3)$), as a proxy measure for the surface adsorbents in the samples, plotted against the cytotoxicity. The analysis was performed for a subset of NGMs with the most graphene-like properties. **e + f** Performance heptagrams representing the NGMs with the lowest and highest cytotoxic profile in **d**. The red line represents the linear fit (**c** and **d**). Deviation bars represent the upper and lower bound for PI.

describes the dimension correlated with WST-1 and LDH. As expected, these two vectors (WST-1 and LDH) point in opposite directions, revealing a negative correlation between them.

An unsupervised HCA was carried out which further confirms the clusters formed in PCA. Five groups were classified for the 36 samples analyzed (Fig. 6b). The largest cluster (in blue) predominantly includes 19 samples, of which 15 are NGM^{int} . Samples in this cluster have the highest principal component score (0–2), which indicates the highest cellular viability and lower cytotoxicity. The second largest cluster (in red) consists of 10 samples, out of which six samples are NGM^{def} . While this cluster has a principal component score comparable to the blue cluster (–1 to 1), it had lower cell proliferation and higher cytotoxicity and grouped separately. The other clusters were cytotoxic with principal component scores of –4 for NGM^{def} (orange) and ranging from –1 to NGM^{int} (green and pink).

DISCUSSION

A precise characterization of graphene-based materials is necessary to anticipate their impact on safety, health, and environment³⁷. We observed that the 36 commercially available NGMs were a diverse class of heterogeneous materials that can be considered either cytocompatible, inert or highly cytotoxic. We found that the carbon content of the sample varies from 63 to 98 wt%. More than a third of the samples contain highly defective graphene, which tends to have a lower carbon content.

Graphene family materials interact with mammalian cells via different mechanisms that may or may not result in toxic effects^{24,27,38–40}. The flow of molecules and materials through the cell membrane is largely dependent on material's particle size, geometry, surface, and molecular chemistries. Particle size exerts strong influence on binding and activation of cellular membrane receptors⁴¹. Dissipative particle dynamics simulations suggest that the interaction of graphene nanosheets (side length of 3.5 nm) with bilayer membrane depends on the material's lateral size and can be divided into three stages: (i) graphene nanosheet draws near to the membrane without a preferred orientation and is not captured by the cell, (ii) the nanosheet assumes an entry angle of $\sim 47^\circ$ while invading the membrane, and (iii) a sandwiched graphene-membrane superstructure is formed upon the rotation of graphene nanosheet towards the center of the lipid bilayer³⁸. Another graphene-cell mode of interaction is material invagination by plasma membrane as observed in protein-coated graphene oxide nanosheets that are engulfed via the formation of intracellular vesicle⁴⁰. Notably, the angles of interaction vary depending on the type of graphene. For instance, protein-coated graphene oxide nanosheets (equivalent diameter of 0.6 μm) adheres face to face, and not perpendicularly, to cell membrane allowing for the formation of intracellular vesicle for engulfment⁴⁰. Conversely, graphene micro-sheets (5–10 μm) can assume acute penetration angles that may pierce and damage cell membranes^{38,42}. It needs to be highlighted that there is no universal size threshold that dictates the internalization and regulates

intracellular distribution of graphene family materials. Nonetheless, it seems that the continuum between small and large particles can change the mode of cellular uptake, from clathrin-mediated endocytosis to phagocytotic uptake, at least for protein-coated graphene oxide nanosheets⁴⁰. Likewise, the manner in which graphene family materials are made available in the microenvironment also influences the mode of interaction with mammalian cells. For instance, films produced with chemically vapor deposited graphene or graphene oxide substrates allow for effective attachment and proliferation of human neurons, cardiomyocytes, and different types of stem cells without apparent adverse effects on cellular and mitochondrial membrane or exacerbation of inflammatory markers^{22,24,25,27,43–48}. On these solid substrates, cells take advantage of material surface features (e.g., wrinkles) to anchor themselves and develop focal adhesion spots^{27,49,50}. In some cases, the chemical and surface features of graphene can even promote cell proliferation due to the higher interaction with secreted-extracellular proteins⁴⁶. It is also possible to modulate cell–substrate adhesion and neurogenic differentiation of human mesenchymal stem cells by changing the size and amount of defects at the domain boundaries of graphene films produced by chemical vapor deposition⁵¹. In summary, the interactions between cells and graphene family materials vary in response to the material's shapes, sizes, chemistries, and modes of use (particle suspension vs. substrates) inducing and modulating several cell responses, including the cell stability, survival, and toxicity.

It has been previously proven that several graphene characteristics (e.g., the presence of functional groups, charges, and sizes) may affect its cytocompatibility²⁸, and our results are consonant with this postulate. Moreover, we demonstrated that no single physical or chemical parameter can define NGMs' cytotoxicity alone. This can be observed in Fig. 1f, wherein NGM-11 and NGM-33 present variable LDH release despite having similar intact structure, high carbon content (≥ 97 wt%), and a low degree of volatile impurities ($\Delta TG < 5\%$). However, NGM-33 presents a lower fraction of sp^2 -bonded carbon ($r(sp^2)$). Meanwhile, NGM-9, which also has a high graphitic content and low $r(sp^2)$, like NGM-33, is more cytocompatible. Strikingly, both NGM-15 and NGM-24 have different cytocompatible characteristics despite having a high density of defects and volatile impurities ($\Delta TG = 21\%$) and low carbon content ($wt\%(C) = 78\%$).

The cytotoxicity was not linked to single parameter that we analyzed. Thus, we have investigated whether the presence of impurities could contribute to the toxicity of commercially available NGMs. We focused on two broad types of impurities, namely persistent inorganics and adsorbents, which can be linked to the purity of the raw graphite and the efficiency of the purification processes performed during the production of NGMs.

First, we observed that the lower bound of PI exceeded 10% of the total sample weight in over 20% of NGMs tested. The PI may be intercalated and adsorbed impurities as well as chemical residues from the synthesis processes^{52–54}. Notably, the trendline from Fig. 6c suggests that NGMs are more cytotoxic as the PI fraction increases ($r_s = 0.393$; $p < 0.05$). The PI exemplifies the negative effects of production residues on the cytotoxicity of commercially available graphene materials.

We have also investigated the effects of impurities (e.g., adsorbents and surfactants) on NGMs' toxicity. For this, we have selected ten NGMs presenting low fraction of volatiles ($\Delta TG < 5\%$), and PI ($< 3.5\%$) and $wt\%(C) > 95\%$ (Fig. 6d). In these samples, most of the anticipated impurities may be carbon-rich surfactants that adsorb on the graphene surface that would decrease the sp^2/sp^3 ratio (Supplementary Fig. 5). Notably, 9 out of 10 samples with the highest sp^3 bond fraction $r(sp^3)$ are NGM^{int}, which confirms the assumption that the NGMs with the most ideal composition rely heavily on surfactants in their method of synthesis¹⁰. This was supported by TGA-MS, as identified cleaved fragments are typical

for aromatic (e.g., $m/z \sim 77$) or aliphatic organic compounds ($m/z \sim 15$ for CH_3 , ~ 29 for C_2H_5), which should be not present in pristine graphene (Supplementary Table 1). There was an insignificant correlation between cytotoxicity (cell membrane rupture) and $r(sp^3)$, which is a measure of the density of graphene adsorbents ($r_s = 0.382$; $p > 0.05$, Fig. 6d). Interestingly, when we compared the least and most toxic samples from this group of NGM^{int}, the sp^2 fraction was the most prominent factor inducing toxicity (Fig. 6e, f). Thus, these non-graphene additives and impurities (possibly from the raw materials or synthesis methods) are likely to increase cytotoxicity. Unfortunately, these compounds are highly specific to the synthesis processes which are rarely disclosed by manufacturers.

There was a statistically significant moderate correlation between PIs and LDH (Fig. 6c) Notably, we have observed a decrease in toxicity after washing the samples to remove persistent inorganics and impurities (Fig. 5a, b). These findings reinforce the need for rigorous characterization; at this stage, post-processing/purification must be considered for graphene materials obtained from commercial parties prior to using them in research and development efforts, and to anticipate their impact on safety, health, and environment^{6,37}.

Furthermore, the cytotoxicity induced by graphene and graphene family materials is concentration dependent. It has been seen that higher concentration of graphene in contact with cells for an extended period significantly releases higher levels of lactate dehydrogenase enzyme indicating loss of plasma membrane integrity³⁹. This is coherent with the results seen in our study whereby higher level of LDH was seen associated with high flake size (LDH ($r_s^{com} = 0.470$, $p < 0.05$, Table 1).

The issue of graphene toxicity must be urgently addressed from two distinct perspectives: the harmonization of experimental protocols and consideration of application specificities. The plethora of testing concentrations used to assess graphene's toxicity, from millimolar to $g\ ml^{-1}$ ^{24,27,28,38–40,42}, renders it impossible to discern what is indeed the toxic character of graphene family materials. Herein, some of the materials tested at $10\ \mu g/ml$ were deemed cytotoxic, whereas no apparent cytotoxic effects have been observed for other graphene family materials tested in other studies at the same concentration⁵⁵. We have also observed that even samples categorized as "cytocompatible" were deemed excessively cytotoxic when tested at $50\ \mu g/ml$, resulting in very high LDH values and eradication of cells (data not shown). Similar detrimental effects at $50\ \mu g/ml$ have been observed, such as increased degrees of LDH release by another type of mammalian cells⁵⁵ and generation of reactive oxygen species (ROS) by microbial communities present in sludge samples from a wastewater treatment plant⁵⁶. Some of these detrimental effects may be associated with graphene family materials altering cell function through the interaction with organelles which can lead to alteration, or overproduction of ROS which is preceded by various factors viz., altered mitochondrial membrane potential, localization of graphene nanoparticles on the F-actin filament or activation of nicotinamide adenine dinucleotide phosphate (NADPH) oxidase system^{57–59}. In our study, we have used WST-1 reagent to study the mitochondrial activity, which is based on the principle of cleavage of tetrazolium salts by viable enzymes from mitochondria (mainly mitochondrial dehydrogenase) to form colored formazans (reported here as absorbance), which are indicative of mitochondrial and thus cellular viability. Notably, the carbon content (analyzed by EA in Fig. 4e) was positively correlated with the mitochondrial activity (WST-1 $r_s^{com} = 0.499$, $p < 0.001$, Table 1). Previous studies have shown that carbon nanoparticles can present positive effects on cell proliferation, viability, and adhesion when grafted over polyethylene polymers^{60,61}. This is coherent with our findings as a higher carbon percentage, despite the lattice arrangement, has

significantly positive correlations and thus the effect on measures of cellular viability (Fig. 4).

The “risk/no-risk” or “toxic/non-toxic” archetypes are no longer acceptable if one does not put into context the intended use of graphene family materials^{6,62}. For instance, graphene films coated on arbitrary materials have been repeatedly proven to be cytocompatible^{21,22,24–26,43,63}. Nonetheless, those findings cannot be proxies to confirm the cytocompatibility of graphene family materials dispersed in suspensions^{6,55,56}. Thus, results from a specific experimental set-up cannot be applied to all potential graphene applications (e.g., coating vs. drug carrier/delivery systems). Likewise, the experimental set-ups also have intrinsic limitations. Herein, we have followed the ISO guidelines that recommend established cell lines from recognized repositories for cytotoxicity tests²⁹. However, immortalized cell lines may present chromosomal instability and metabolic abnormalities due to their derivation. Alternatively, primary and stem cells have brief lifespans, can lose specific markers over short time in culture, and present varied genomic profiles depending on the donor; all of which can influence the cell’s biological response to materials⁶⁴. Herein, the trend observed in the cytotoxic character of selected NGMs characterized with immortalized cell lines (L929) was similar to that observed with human mesenchymal stem cells despite the numerical variations observed for the absorbance values (Supplementary Fig. 10). This data, therefore, suggests that not only cytotoxicity is material-specific, but also NGMs may present varying toxicity levels depending on the type of cells and tissues analyzed (as previously shown in^{6,65,66}).

We also need to highlight that the characterizations and assays performed in our study are non-exhaustive and overlook certain properties like surface charge and graphene shape (sharpness) that can also affect cell membrane integrity and overall toxicity profile^{42,67}. We have also observed that safety datasheets provided by graphene suppliers are either unavailable or inadequate, reflecting the urgent need for the establishment of standards for quality assurance and the communication of technical information for commercial graphene products. Hence, it is critical to establish the basic testing standards to which a graphene sample needs to be subjected to characterize its safety and biocompatibility. The fast-paced scientific breakthroughs and anticipation of graphene products with enhanced capabilities have great potential to transform many industries. However, not all institutes and enterprises involved in graphene research and development are fully equipped to independently produce and characterize high-quality graphene materials. Hence, using materials that are commercially available becomes a mean to advance research efforts. This scenario is promoting the emergence of new and much-needed type of industry that aims to make graphene materials readily available worldwide. The use of commercially available samples has allowed advancing research efforts, but the lack of international standards and specifications (viz. assessing cytocompatibility) could precipitate severe reluctance and delays in the implementation of new technologies.

Our work showed that over than 35% of commercially available graphene materials were defective graphene layers as determined by Raman and XPS analysis and that no single property or characteristic can depict enough information about the material’s cytotoxic profile. Moreover, some of the marketed NGM showed persistent impurities that had contributed to higher cytotoxicity. In fact, further purification has reduced the %cytotoxicity by at least 30% in three out of four highly cytotoxic NGM tested. Hence, the structure, purity, and toxicity of commercially available NGM must be independently characterized by customers (researchers). Finally, the high versatility of NGM and diverse potential applications demand the biological outcomes to be interpreted in the light of intended final graphene-based/-containing product.

METHODS

Sample preparation and characterization

We obtained 36 commercially available graphene samples from graphene producers located in the United States, Canada, India, China, Malaysia, Norway, Italy, and England. Graphene samples in powder form were used in the experiments as received, while graphene dispersions were dried to obtain the powder⁵.

The materials were characterized through the following techniques: CHNS combustion elemental analysis (EA), thermogravimetric analysis coupled with mass spectrometry (TGA-MS), Raman, and X-ray photoelectron spectroscopy (XPS), and light and atomic force microscopy (AFM). The specific surface area (SSA) was determined according to Brunauer, Emmett, and Teller (BET). Bulk samples were used for TGA-MS and EA, while for XPS, Raman, BET, and AFM dispersions of 1 mg/ml were prepared with either water, isopropanol or n-methyl-2-pyrrolidone, and subsequently spin-coated on 300 nm SiO₂/Si wafer (SPS-Europe, 5000 RPM, 90 s).

Carbon content was quantified using carbon, hydrogen, and nitrogen elemental analysis (Elementar Vario MICRO Cube, Germany). A thermogravimetric analyzer coupled with mass spectrometry (STA 449 F3 Jupiter coupled to an Aeolos III mass spectrometer, Netzsch, Germany) was used to characterize the degree of functionalization and contamination in 10 mg of each graphene sample under a helium atmosphere. The relative mass loss was determined as being between 50 °C and 800 °C, and cleaved fragments with *m/z* between 10 and 110 were recorded over the same range. As reference samples, we used graphite (type 3061, Asbury Carbon Mills, USA) or graphene oxide produced from this graphite according to previously published method⁶⁸. We defined a lower bound for the cases in which all the volatiles ΔTG are inorganics ($PI_{low} = 100\% - wt\%(C) - \Delta TG$), and an upper bound if all volatiles are carbon ($PI_{up} = 100\% - wt\%(C)$). Raman spectroscopy (CRM 200, Witec, Germany) was conducted using a green laser with an excitation wavelength of 532 nm and a 100× objective. For each sample, at least ten different areas were analyzed by recording single spectra with a laser spot size of about 400 nm. The chemical composition was analyzed via X-ray photoelectron spectroscopy (Kartos Analytical Ltd., U.K.) using an Al K α X-ray photon source with $h = 1486.71$ eV. The characteristic carbon peak at 284.8 eV was used as a reference for all binding energies. The degree of functionalization or contamination of each graphene sample was determined by the deconvolution of the Carbon 1s core level spectra and by analyzing the sp^2 and sp^3 contents⁵. We defined the sp^3 bond fraction, $r(sp^3) = 100\% - r(sp^2)$, as a statistical measure of the density of impurities on clean and intact graphene. The SSA of materials was determined using the BET method, and at least ten areas on the SiO₂/Si-wafer were measured.

Flake thickness was determined using atomic force microscopy (Dimension® Icon™ Atomic Force equipped with ScanAsyst™, Bruker, Germany) in tapping mode to study the flake thickness, and the number of layers was estimated as the flake thickness/inter-layer distance. Here, the inter-layer distance was assumed to be the same, with a graphite inter-layer distance of 0.335 nm⁴³. The lateral dimensions of NGMs and their distribution were extracted from light microscopy images with the open-source software ImageJ (version 1.53d, NIH, USA). Therefore, we converted the green channel of the RGB images to a black and white image and analyzed at least 1000 flakes from 10 different areas all over the wafer.

Purification to remove persistent adsorbents and inclusions was performed for selected NGMs by washing with 1 M HCl, followed by ethanol, chloroform, ethanol, 0.1 M KOH (60 °C, 2 h each), and distilled water. The materials were centrifuged between each solution and finally dried at 80 °C at reduced pressure for 48 h.

Cell culture, cytotoxicity, and membrane damage assays

The cytotoxicity of the samples was evaluated following the BS EN ISO Biological evaluation of medical devices Part 5: Tests for in vitro cytotoxicity (ISO 10993-5:2009). To this end, L929 cells (Sigma-Aldrich, USA) were sub-cultured in basal growth media (high-glucose media, 10% fetal bovine serum, and 1% penicillin/streptomycin, all from Gibco, USA) until 70–80% confluence had been reached. Thereafter, cells were harvested (TrypLE, Gibco), seeded in a 96-well plate (10³ cells per well), and left undisturbed for 24 h at 37 °C and 5% CO₂. Subsequently, the basal growth media was completely removed, and the cells were washed with phosphate-buffered solution (PBS, pH 7.4, Gibco). Next, the cells were treated with graphene-containing media which was prepared via mild ultra-sonication of the graphene powder (10 or 25 $\mu\text{g/ml}$) into basal growth culture media for 10 min at room temperature. After the 24 h treatment period, cells were washed twice with PBS.

Cell viability was assessed via WST-1 assay (Abcam, UK), which indicates the proportional number of living cells based on the cleavage of the tetrazolium salt to formazan by cellular mitochondrial dehydrogenase, enabling estimates of the relative number of living cells. To this end, cells were treated with 100 μ l of fresh basal growth media containing 10 μ l WST-1 reagent for 90 min at 37 °C. Afterwards, 70 μ l of media was transferred to a new plate, and the absorbance was taken at 450 nm (Multiskan GO, ThermoFischer, USA).

Cytotoxicity was assessed based on cell membrane damage, which was quantified by the release of LDH. For this, CytoTox-One (Promega, USA) and supernatant basal growth media were mixed (50 μ l each), added to the wells, and incubated at room temperature for 30 min. Following the incubation, the fluorescence was measured at 560_{Ex}/590_{Em} (Fluoroskan FL, ThermoFischer, USA), and the percentage of cytotoxicity was calculated using Eq. (1).

$$\%_{\text{cytotoxicity}} = 100 * \left(\frac{\text{Experimental} - \text{Culture medium background}}{\text{Maximum LDH release} - \text{Culture medium background}} \right) \quad (1)$$

The negative control was cells cultured in basal growth media without NGMs, and the positive control for LDH was cells pre-treated with lysis buffer. All the cellular toxicity experiments were performed in three independent sessions.

Statistical analysis

The potential association of tested properties and cell viability and cytotoxicity was analyzed using a bivariate Spearman correlation analysis (SPSS version 22.0, IBM, USA). The Spearman's correlation coefficient (r_s), along with the probability value (p), are reported. We also report the median (50th) along with 10th to 90th percentile values of the assessed parameters.

PCA was performed for cell viability and cytotoxicity, reported as WST-1 and LDH at 10 μ g/ml after centering the data obtained with different units and scales. The number of principal components was selected according to Kaiser's criterion and using a scree plot. Only principal components with Eigenvalue greater than 1 were retained. The score and loading plot were drawn. The principal component score was computed to represent the cytocompatibility of the samples.

An unsupervised HCA was employed to establish clusters among the samples based on toxicity. Clusters were formed through the agglomerative process, starting with connecting two samples with the highest similarities. The Euclidean distance with the average linkage method was used to compute the samples' similarities. A circular dendrogram was plotted to present the result of the hierarchical clustering analysis. The vertical lines in the dendrogram represent root samples, while horizontal lines represent similarities between samples in terms of Euclidean distance. The PCA and HCA were performed using multivariate analysis in Origin (2019(b), OriginLab, USA).

DATA AVAILABILITY

The datasets generated during and/or analyzed during the current study are available from the corresponding author on reasonable request.

Received: 23 October 2021; Accepted: 13 July 2022;

Published online: 09 September 2022

REFERENCES

- Dreyer, D. R., Todd, A. D. & Bielawski, C. W. Harnessing the chemistry of graphene oxide. *Chem. Soc. Rev.* **43**, 5288–5301 (2014).
- Homaeigohar, S. & Elbahri, M. Graphene membranes for water desalination. *NPG Asia Mater.* **9**, e427 (2017).
- Malhotra, R. et al. Graphene nanocoating provides superb long-lasting corrosion protection to titanium alloy. *Dent. Mater.* **37**, <https://doi.org/10.1016/j.dental.2021.08.004> (2021).
- Luong-Van, E. K., Madanagopal, T. T. & Rosa, V. Mechanisms of graphene influence on cell differentiation. *Mater. Today. Chem.* **16**, <https://doi.org/10.1016/j.mtchem.2020.100250> (2020).
- Kauling, A. P. et al. The worldwide graphene flake production. *Adv. Mater.* **30**, 1803784 (2018).
- Xie, H., Cao, T., Rodriguez-Lozano, F. J., Luong-Van, E. K. & Rosa, V. Graphene for the development of the next-generation of biocomposites for dental and medical applications. *Dent. Mater.* **33**, 765–774 (2017).
- Zhang, Z., Fraser, A., Ye, S., Merle, G. & Barralet, J. Top-down bottom-up graphene synthesis. *Nano Futures* **3**, <https://doi.org/10.1088/2399-1984/ab4eff> (2019).
- Ambrosi, A. et al. Metallic impurities in graphenes prepared from graphite can dramatically influence their properties. *Angew. Chem. Int. Ed.* **51**, 500–503 (2012).
- Ambrosi, A. et al. Chemically reduced graphene contains inherent metallic impurities present in parent natural and synthetic graphite. *PNAS* **109**, 12899–12904 (2012).
- Backes, C. et al. Production and processing of graphene and related materials. *2D Mater.* **7**, 022001 (2020).
- Hummers, W. S. Preparation of graphitic acid. US2798878 (US2798878, 1957).
- Parvez, K. et al. Exfoliation of graphite into graphene in aqueous solutions of inorganic salts. *J. Am. Chem. Soc.* **136**, 6083–6091 (2014).
- Xu, J. et al. Liquid-phase exfoliation of graphene in organic solvents with addition of naphthalene. *J. Colloid Interface Sci.* **418**, 37–42 (2014).
- Coleman, J. N. Liquid exfoliation of defect-free graphene. *Acc. Chem. Res.* **46**, 14–22 (2013).
- Paton, K. R. et al. Scalable production of large quantities of defect-free few-layer graphene by shear exfoliation in liquids. *Nat. Mater.* **13**, 624–630 (2014).
- Hernandez, Y. et al. High-yield production of graphene by liquid-phase exfoliation of graphite. *Nat. Nanotechnol.* **3**, 563–568 (2008).
- Gurunathan, S., Kang, M.-H., Jeyaraj, M. & Kim, J.-H. Differential cytotoxicity of different sizes of graphene oxide nanoparticles in Leydig (TM3) and Sertoli (TM4) cells. *Nanomaterials* **9**, <https://doi.org/10.3390/nano9020139> (2019).
- Hofer, C. et al. Direct imaging of light-element impurities in graphene reveals triple-coordinated oxygen. *Nat. Commun.* **10**, <https://doi.org/10.1038/s41467-019-12537-3> (2019).
- Feicht, P. & Eigler, S. Defects in graphene oxide as structural motifs. *ChemNanoMat* **4**, 244–252 (2018).
- Gómez-Navarro, C. et al. Atomic structure of reduced graphene oxide. *Nano Lett.* **10**, 1144–1148 (2010).
- Xie, H., Cao, T., Gomes, J. V., Castro Neto, A. H. & Rosa, V. Two and three-dimensional graphene substrates to magnify osteogenic differentiation of periodontal ligament stem cells. *Carbon* **93**, 266–275 (2015).
- Kalbacova, M., Broz, A., Kong, J. & Kalbac, M. Graphene substrates promote adherence of human osteoblasts and mesenchymal stromal cells. *Carbon* **48**, 4323–4329 (2010).
- Morin, J. L. P. et al. Graphene transfer to 3-dimensional surfaces: a vacuum-assisted dry transfer method. *2D Mater.* **4**, 025060 (2017).
- Dubey, N. et al. Graphene onto medical grade titanium: an atom-thick multimodal coating that promotes osteoblast maturation and inhibits biofilm formation from distinct species. *Nanotoxicology* **12**, 274–289 (2018).
- Xie, H., Cao, T., Franco-Obregón, A. & Rosa, V. Graphene-induced osteogenic differentiation is mediated by the integrin/FAK axis. *Int. J. Mol. Sci.* **20**, 574 (2019).
- Nayak, T. R. et al. Graphene for controlled and accelerated osteogenic differentiation of human mesenchymal stem cells. *ACS Nano* **5**, 4670–4678 (2011).
- Rosa, V. et al. Graphene oxide-based substrate: physical and surface characterization, cytocompatibility and differentiation potential of dental pulp stem cells. *Dent. Mater.* **32**, 1019–1025 (2016).
- Yang, K., Li, Y., Tan, X., Peng, R. & Liu, Z. Behavior and toxicity of graphene and its functionalized derivatives in biological systems. *Small* **9**, 1492–1503 (2013).
- International Organization for Standardization (ISO). in *Nanotechnologies – Vocabulary* (ed. BSI Standards Publication) (2017).
- Bianco, A. et al. All in the graphene family—a recommended nomenclature for two-dimensional carbon materials. *Carbon* **65**, 1–6 (2013).
- Wick, P. et al. Classification framework for graphene-based materials. *Angew. Chem. Int. Ed. Engl.* **53**, 7714–7718 (2014).
- Cancado, L. G. et al. Quantifying defects in graphene via Raman spectroscopy at different excitation energies. *Nano Lett.* **11**, 3190–3196 (2011).
- Vecera, P. et al. Degree of functionalisation dependence of individual Raman intensities in covalent graphene derivatives. *Sci. Rep.* **7**, <https://doi.org/10.1038/srep45165> (2017).
- Kozhemyakina, N. V. et al. Effect of the structure and morphology of natural, synthetic and post-processed graphites on their dispersibility and electronic properties. *Fuller. Nanotub. Carbon Nanostruct.* **21**, 804–823 (2013).
- Kovtun, A. et al. Accurate chemical analysis of oxygenated graphene-based materials using X-ray photoelectron spectroscopy. *Carbon* **143**, 268–275 (2019).
- Gengenbach, T. R., Major, G. H., Linford, M. R. & Easton, C. D. Practical guides for x-ray photoelectron spectroscopy (XPS): Interpreting the carbon 1s spectrum. *J. Vac. Sci. Technol.* **39**, <https://doi.org/10.1116/6.0000682> (2021).
- Fadeel, B. et al. Safety assessment of graphene-based materials: focus on human health and the environment. *ACS Nano* **12**, 10582–10620 (2018).

38. Guo, R., Mao, J. & Yan, L.-T. Computer simulation of cell entry of graphene nanosheet. *Biomaterials* **34**, 4296–4301 (2013).
39. Li, Y. et al. Response of microRNAs to in vitro treatment with graphene oxide. *ACS Nano* **8**, 2100–2110 (2014).
40. Mu, Q. et al. Size-dependent cell uptake of protein-coated graphene oxide nanosheets. *ACS Appl. Mater. Interfaces* **4**, 2259–2266 (2012).
41. Jiang, W., Kim, B. Y. S., Rutka, J. T. & Chan, W. C. W. Nanoparticle-mediated cellular response is size-dependent. *Nat. Nanotechnol.* **3**, 145–150 (2008).
42. Li, Y. et al. Graphene microsheets enter cells through spontaneous membrane penetration at edge asperities and corner sites. *PNAS* **110**, 12295–12300 (2013).
43. Rosa, V. et al. Graphene nanocoating: high quality and stability upon several stressors. *J. Dent. Res.* **100**, 1169–1177 (2021).
44. Park, J. et al. Graphene-regulated cardiomyogenic differentiation process of mesenchymal stem cells by enhancing the expression of extracellular matrix proteins and cell signaling molecules. *Adv. Healthc. Mater.* **3**, 176–181 (2014).
45. Lee, J. S. et al. Graphene substrate for inducing neurite outgrowth. *Biochem. Biophys. Res. Commun.* **460**, 267–273 (2015).
46. Rastogi, S. K., Raghavan, G., Yang, G. & Cohen-Karni, T. Effect of graphene on nonneuronal and neuronal cell viability and stress. *Nano Lett.* **17**, 3297–3301 (2017).
47. Xie, H. et al. CVD-grown monolayer graphene induces osteogenic but not odontoblastic differentiation of dental pulp stem cells. *Dent. Mater.* **33**, e13–e21 (2017).
48. Madanagopal, T. T. et al. Pulsed electromagnetic fields synergize with graphene to enhance dental pulp stem cell-derived neurogenesis by selectively targeting TRPC1 channels. *Eur. Cell. Mater.* **41**, 216–232 (2021).
49. Jeong, J.-T. et al. Effect of graphene oxide ratio on the cell adhesion and growth behavior on a graphene oxide-coated silicon substrate. *Sci. Rep.* **6**, <https://doi.org/10.1038/srep33835> (2016).
50. Sun, L. et al. Graphene-based 2D constructs for enhanced fibroblast support. *PLoS One* **15**, <https://doi.org/10.1371/journal.pone.0232670> (2020).
51. Lee, Y.-J. et al. Neuronal differentiation of human mesenchymal stem cells in response to the domain size of graphene substrates. *J. Biomed. Mater. Res. A* **106**, 43–51 (2018).
52. Viculis, L. M., Mack, J. J., Mayer, O. M., Hahn, H. T. & Kaner, R. B. Intercalation and exfoliation routes to graphite nanoplatelets. *J. Mater. Chem.* **15**, 974–978 (2005).
53. Zhan, D. et al. FeCl₃-based few-layer graphene intercalation compounds: single linear dispersion electronic band structure and strong charge transfer doping. *Adv. Funct. Mater.* **20**, 3504–3509 (2010).
54. Kalucki, K. & Morawski, A. W. Iron intercalated in graphite as catalysts for ammonia synthesis. *J. Chem. Technol. Biotechnol.* **47**, 357–363 (2007).
55. Chang, Y. et al. In vitro toxicity evaluation of graphene oxide on A549 cells. *Toxicol. Lett.* **200**, 201–210 (2011).
56. Ahmed, F. & Rodrigues, D. F. Investigation of acute effects of graphene oxide on wastewater microbial community: a case study. *J. Hazard. Mater.* **256–257**, 33–39 (2013).
57. Matesanz, M. C. et al. The effects of graphene oxide nanosheets localized on F-actin filaments on cell-cycle alterations. *Biomaterials* **34**, 1562–1569 (2013).
58. Li, Y. et al. The triggering of apoptosis in macrophages by pristine graphene through the MAPK and TGF-beta signaling pathways. *Biomaterials* **33**, 402–411 (2012).
59. Xiaoli, F. et al. Graphene oxide disrupted mitochondrial homeostasis through inducing intracellular redox deviation and autophagy-lysosomal network dysfunction in SH-SY5Y cells. *J. Hazard. Mater.* **416**, 126158 (2021).
60. Zakova, P. et al. Cytocompatibility of amine functionalized carbon nanoparticles grafted on polyethylene. *Mater. Sci. Eng. C. Mater. Biol. Appl.* **60**, 394–401 (2016).
61. Švorčík, V. et al. Cytocompatibility of polymers grafted by activated carbon nanoparticles. *Carbon* **69**, 361–371 (2014).
62. Arvidsson, R., Boholm, M., Johansson, M. & de Montoya, M. L. “Just Carbon”: ideas about graphene risks by graphene researchers and innovation advisors. *NanoEthics* **12**, 199–210 (2018).
63. Li, K. et al. Evaluation of the osteogenesis and osseointegration of titanium alloys coated with graphene: an in vivo study. *Sci. Rep.* **8**, <https://doi.org/10.1038/s41598-018-19742-y> (2018).
64. Rosa, V., Toh, W. S., Cao, T. & Shim, W. Inducing pluripotency for disease modeling, drug development and craniofacial applications. *Expert Opin. Biol. Ther.* **14**, 1233–1240 (2014).
65. Tabish, T. A. et al. Investigation into the toxic effects of graphene nanopores on lung cancer cells and biological tissues. *Appl. Mater. Today* **12**, 389–401 (2018).
66. Agarwal, S. et al. Interfacing live cells with nanocarbon substrates. *Langmuir* **26**, 2244–2247 (2010).
67. Wang, A. et al. Role of surface charge and oxidative stress in cytotoxicity and genotoxicity of graphene oxide towards human lung fibroblast cells. *J. Appl. Toxicol.* **33**, 1156–1164 (2013).
68. Nacken, T. J. et al. Structural factors controlling size reduction of graphene oxide in liquid processing. *Carbon* **125**, 360–369 (2017).

ACKNOWLEDGEMENTS

We thank Alan Kauling for levelheaded discussions. This work has been supported by grants from the Ministry of Education, Singapore Academic Research Fund Tier 1 grant A-0002091-00-00 (V.R.), Ministry of Education, Singapore Academic Research Fund Tier 1 grant R-221-000-132-114 (V.R.), National University Health System, Singapore grant NUHS Open Collaborative Research Grant NUHS O-CRG 2016 Oct-25 (V.R.), National Research Foundation, Prime Minister's Office, Singapore grant Award No. NRF2014NRF-CRP001-024 (G.S.) National Research Foundation, Prime Minister's Office, Singapore grant (A.H.C.N.).

AUTHOR CONTRIBUTIONS

R.M. and C.E.H. are co-first authors and have contributed equally to this work. Conceptualization: V.R., S.G., A.H.C.N.; Methodology: V.R., D.T.W.L., G.S., R.M., C.E.H.; Investigation: V.R., R.M., C.E.H.; Resources: V.R., D.T.W.L., C.T.L., S.G., A.H.C.N.; Discussions: V.R., R.M., C.E.H., S.G.; Writing—original draft: V.R., R.M., C.E.H., S.G.; Writing—review & editing: R.M., C.E.H., D.T.W.L., C.T.L., A.H.C.N., S.G., V.R.; Supervision: V.R.; Funding acquisition: A.H.C.N., S.G., and V.R.

COMPETING INTERESTS

A.H.C.N. declares the following Competing Financial Interest: founder and shareholder of 2D Materials Pte. Ltd. All the other authors declare no competing financial or non-financial interests.

ADDITIONAL INFORMATION

Supplementary information The online version contains supplementary material available at <https://doi.org/10.1038/s41699-022-00330-8>.

Correspondence and requests for materials should be addressed to A. H. Castro Neto, Slaven Garaj or Vinicius Rosa.

Reprints and permission information is available at <http://www.nature.com/reprints>

Publisher's note Springer Nature remains neutral with regard to jurisdictional claims in published maps and institutional affiliations.



Open Access This article is licensed under a Creative Commons Attribution 4.0 International License, which permits use, sharing, adaptation, distribution and reproduction in any medium or format, as long as you give appropriate credit to the original author(s) and the source, provide a link to the Creative Commons license, and indicate if changes were made. The images or other third party material in this article are included in the article's Creative Commons license, unless indicated otherwise in a credit line to the material. If material is not included in the article's Creative Commons license and your intended use is not permitted by statutory regulation or exceeds the permitted use, you will need to obtain permission directly from the copyright holder. To view a copy of this license, visit <http://creativecommons.org/licenses/by/4.0/>.

© The Author(s) 2022